Extensor Digitorum Communis Compartments With a Double Compensation Synergy Strategy for Constant Force Control of the Index Finger

Zhixian Gao, Yehong Zhang, Yun Zhao, Yinping Wei, Shiyang Lv, Zhenpeng Shao, Zongya Zhao, Chang Wang, Xuezhi Zhou, Junqiang Zhao, Wensheng Hou, and Yi Yu

***Abstract*— Precise sustained force control of the fingers is important for achieving flexible hand movements. However, how neuromuscular compartments within a forearm multi-tendon muscle cooperate to achieve constant finger force remains unclear. This study aimed to investigate the coordination strategies across multiple compartments of the extensor digitorum communis (EDC) during index finger sustained constant extension. Nine subjects performed index finger extensions of 15%, 30%, and 45% maximal voluntary contractions, respectively. High-density surface electromyography signals were recorded from the EDC and then analyzed using non-negative matrix decomposition to extract activation patterns and coefficient curves of EDC compartments. The results showed two activation patterns with stable structures during all tasks: one pattern corresponding to the index finger compartment was named primary pattern; whereas the other corresponding to other compartments was named auxiliary pattern. Further, the intensity and stability of their coefficient curves were assessed using the root mean square value (RMS) and coefficient of variation (CV). The RMS and CV values of the primary pattern increased and decreased with time, respectively, while the corresponding values of the auxiliary pattern were both negatively correlated with the formers. These findings suggested a special coordination strategy across EDC compartments during index finger constant extension, manifesting as two compensations of the auxiliary pattern for the intensity and stability of the primary pattern. The proposed method provides new insight into the synergy strategy across multiple compartments within a forearm multi-tendon during sustained isometric contraction of a single finger and a new approach for constant force control of prosthetic hands.**

***Index Terms*— High-density surface electromyography, neuromuscular compartments, multi-tendon muscle, synergy, extensor digitorum communis.**

Manuscript received 4 October 2022; revised 13 February 2023; accepted 16 February 2023. Date of publication 22 February 2023; date of current version 28 February 2023. This work was supported in part by the Key-Area Research and Development Program of Guangdong Province under Grant 2020B0909020004, in part by the Science and Technology Research Project of Henan Province under Grant 212102310892, in part by the Science and Technology Research Program Project of Xinxiang City under Grant GG2021013, and in part by the Major Science and Technology Special Projects of Henan Province under Grant 221100310500. *(Corresponding authors: Wensheng Hou; Yi Yu.)*

This work involved human subjects or animals in its research. Approval of all ethical and experimental procedures and protocols was granted by the Ethics Committee of Chongqing Cancer Hospital and performed in line with the Declaration of Helsinki.

Zhixian Gao, Yehong Zhang, Zongya Zhao, Chang Wang, Xuezhi Zhou, Junqiang Zhao, and Yi Yu are with the School of Medical Engineering and the Engineering Technology Research Center of Neurosense and Control of Henan Province, Xinxiang Medical University, Xinxiang 453004, China, and also the Henan International Joint Laboratory of Neural Information Analysis and Drug Intelligent Design, Xinxiang 453004, China (e-mail: yuyi@xxmu.edu.cn).

Yun Zhao is with the School of Smart Health, Chongqing College of Electronic Engineering, Chongqing 401333, China.

Yinping Wei, Shiyang Lv, and Zhenpeng Shao are with the School of Medical Engineering and the Engineering Technology Research Center of Neurosense and Control of Henan Province, Xinxiang Medical University, Xinxiang 453004, China.

Wensheng Hou is with the Key Laboratory of Biorheological Science and Technology, Ministry of Education, Bioengineering College, Chongqing University, Chongqing 400044, China (e-mail: w.s.hou@cqu.edu.cn).

Digital Object Identifier 10.1109/TNSRE.2023.3247141

I. Introduction

THE human hand can manipulate objects flexibly, which requires not only a high degree of single-finger dexterity but also precise force control by the coordination of multiple fingers [1], [2]. In fact, even the force of a single finger is not completely independent of other fingers [3]. This is attributed to the different compartments of forearm multi-tendon muscles that control finger actions having anatomical and neural connections, such as inter-tendinous connections [3], [4], common synaptic input [5], [6], multidigit motor units [7], and the overlap of activation regions in the motor cortex [8]. These complex connections of the multi-tendon muscles provide the physiological basis for finger coordination [2], [9]. Growing evidence showed that the central nervous system (CNS) simplifies the control of the complex sensorimotor system through organizing and regulating low-dimensional coordinative structures (referred to as synergies, modes, or modules) that work together to produce a desired effect [10], [11], [12]. Previous studies investigated finger force control commonly at several levels of the motor hierarchy, such as joints, muscles, and digital forces [13]. Recent studies extended the multiple hierarchies of the sensorimotor system to more levels: up to motor neuron synergies across multiple muscle compartments [14], [15] and down to motor unit modes inside a single

muscle with multiple compartments [16]. Noteworthy, as a sub-muscular level, muscle compartments are not synonymous with motor unit modes [17]. Therefore, it is deserved to further investigate coordination strategies for finger force control at the level of compartments.

As an extrinsic hand muscle, the main role of the forearm multi-tendon muscle is to provide the output force for the fingers [18]. Based on the complex connections mentioned above, both the compartments of the instructed and non-instructed fingers are involved in the digit force control. Previous studies have applied kinetics to investigate the coordination of instructed and non-instructed fingers and found two patterns of finger interaction, enslaving [19] and error compensation [20]. Enslaving occurs when the non-instructed finger is involved in a pressing task with a low force level (<10%MVC) [19]. The force generated by the non-instructed fingers is a positive correlation with the primary force [21]. Error compensation is characterized by the negative correlation between the instructed and non-instructed fingers [22], which is considered to be an essential feature of motor synergies [23]. These results confirmed the existence of kinetic synergies when generating finger forces, even the force output of a finger should also be achieved by multi-finger kinetic synergies [24], [25], [26]. However, kinetic synergies are obtained from multi-finger forces and are considered as resulting from muscle synergies [27]. The collaboration of multiple compartments for finger force control has not yet been studied based on muscle synergy. Therefore, it is necessary to perform essential research on finger force control from the perspective of coordination across multiple compartments.

As an electrophysiology signal of muscle activation, surface electromyography (sEMG) signals have been wildly used in studying muscle coordination [28], [29]. In related studies, a single muscle is considered to be uniformly activated and its sEMG signal is usually recorded using a bipolar electrode pair placed over the muscle belly [30]. However, a bipolar electrode could not fully capture the global information of a multi-tendon muscle [31]. Even if multiple bipolar electrodes are placed over each compartment according to the anatomy, only local information about the compartment is obtained. Moreover, for the slender compartments of forearm multi-tendon muscles, such as the extensor digitorum communis (EDC), it is difficult to avoid sEMG signal crosstalk from adjacent compartments [32]. High-density (HD) sEMG records the bi-dimensional spatial activation information of target muscles [33] using an array with dozens or hundreds of unipolar electrodes [34], which allows insights into the activation of different compartments of multi-tendon muscles [35], [36]. Based on HD sEMG, previous studies have investigated the primary active regions or spatial activation patterns of multi-tendon muscles during dynamic or static movements. Hu et al. obtained the global spatial activation patterns of EDC by the root mean squared (RMS) grid map, localized the centroid marks of the maps during individual finger extensions, and found the muscle active map was relatively consistent across conditions(dynamic or static and high or low effort) [37]. Using the global RMS maps, Dai et al. also extracted the unique spatial patterns of the forearm flexor during individual finger flexions at 30% and 60%MVC, and obtained high classified accuracy using pattern recognition based on the features of these maps [34]. Indeed, RMS maps used by these studies represent the global spatial activation of different compartments during individual finger movements, which ignored the different activation patterns across multiple compartments. Beek et al. assessed the activation of the flexor digitorum superficialis (FDS) and the EDC during single finger flexion and found considerable active regions of the muscles associated with the non-instructed fingers [3]. We previously investigated the changes in the spatial activation distribution of the EDC during continuous extension of the index finger and found different regions of the maps, where the activation intensity has a specific range of variation, were adjusted with a specific regularity [38]. The results suggest that, during sustained single-finger extension, the compartments may play different roles to coordinate precise control tasks. Hence, it is necessary to further investigate whether there are coordination patterns of instructed and non-instructed fingers in the EDC compartments and their corresponding motor control strategies during sustained isometric contraction of the index finger.

In recent years, some studies utilized factorization algorithms to extract the spatiotemporal activation patterns of a single compartment. The non-negative matrix decomposition (NMF) method was shown to be able to cluster the channels with similar profiles of temporal activation from the HD sEMG signals, which has been successfully applied to locate the active region of the compartments within biceps brachii and gastrocnemius [33]. The obtained invariant patterns of muscle activity can exhibit the location of compartments, and the corresponding time-varying coefficients can depict the variation of compartment activation level during dynamic motion tasks, which provide objective information on the spatiotemporal characteristics of activation regions. Given that the "muscle synergies" means that multiple muscles can be activated as a small number of stable units by changing their timing and/or neural drive [39]. Hence, we hypothesized that to simplify the finger force control: (1) the stable coordination patterns of instructed and non-instructed fingers exist in EDC compartments; and (2) the patterns should be regulated by different coordination control strategies during sustained isometric contraction of a single finger. In this study, nine subjects were instructed to perform sustained isometric extensions of the index finger at three force levels. sEMG signals from EDC were recorded by an HD electrode array during the tasks and analyzed by the NMF method to extract activation patterns and coefficient curves of EDC compartments. The intensity and stability characteristics of coefficient curves were proposed to explore the coordination process of EDC compartments during sustained contraction.

II. Methods

A. Subjects

Nine healthy subjects (mean age: 24±1.2 years) were recruited for this study. Subjects had no history of exercise-related neurological and skeletal muscle disease and no

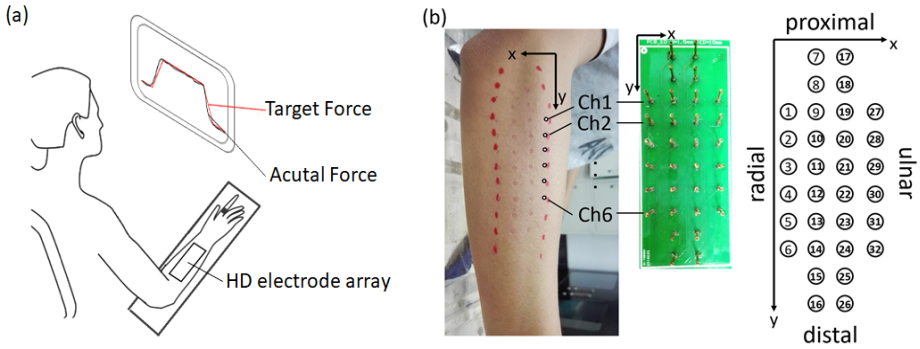

Fig. 1. (a) The scene of the task for sustained force-tracking during right index finger extension. (b) The sEMG signals of ED (red marker) were recorded with a custom-made HD electrode array.

participation in high-intensity activity within two days before the experiment. All of them were right-handed according to their hand use during writing and eating in daily activities, and had normal or corrected to normal vision. The experiment was approved by the local ethical review committee. All subjects gave written informed consent before the experiment.

B. Experimental Protocol

Subjects sat in a chair comfortably, with the right forearm placed on a horizontal shelf. Their elbow joints were maintained at 120°. To minimize crosstalk from wrist muscle activity, their wrists were in a neutral horizontal position, which remained stable during the experiment. The proximal phalanx of the index finger was placed in the ring of a customized force transducer (JLBS-5kg, Bengbu Sensor Company, Bengbu, China) to measure finger force, and other fingers were kept relaxed, as shown in Fig. 1a.

The maximum voluntary contraction (MVC) of the subject's index finger was measured before performing tasks. 3-second MVCs were performed three times and the largest one was selected as the final MVC value. A 5-minute rest was taken to avoid fatigue. The force-tracking tasks were conducted at 15%, 30%, and 45% MVC. Subjects extended the right index finger to track the target force curve on a screen and held the force for the 90s as smoothly as possible. Each task was repeated 3 times with a 10-minute interval. The practice allowed for the subjects to be familiar with the tasks before the formal test.

C. Signal Acquisition

To avoid arrays covering adjacent muscles, the sEMG signals from the EDC were acquired via a homemade 32-channel sEMG array with a 10 mm interval-electrode distance (Fig. 1b). According to the EDC shape, wide in the middle and narrow at both ends, the array was designed as a matrix with 4 columns, containing 6, 10, 10, and 6 electrodes, respectively. Moreover, we chose electrode probes with a cup-shaped head to prevent the spill of conductive paste caused by pressing when placing the array, which ensures a reliable range of the recorded signals. To accurately place the electrode array, the edge of the EDC muscle was identified by ultrasonography (DC-8, Mindray, Shenzhen, China). The ultrasound probe was moved over the skin above the EDC and its edges were marked with a red marker when detected, outlining the muscle portion of the EDC (excluding the anterior and posterior ends of the tendon portion). Then, the vertical and horizontal midlines of the array are aligned with the vertical and horizontal midlines of the marked muscle portion, respectively [39]. Before placing the electrode array, the skin was shaved with abrasive paste and cleaned with medical alcohol. The electrode array was fixed to the forearm with medical tape. The sEMG signals and force data were sampled by Cerebus (BlackRock MicroSystem, Salt Lake City, Utah, USA) at 2000 Hz and a gain of 300 times.

D. Data Analysis

As shown in Fig. 2, the data analysis was performed to investigate the synergistic strategy of EDC compartments. Firstly, the envelopes were extracted from the pre-processed 32-channel sEMG signal, and the NMF method was used to extract the synergy patterns and corresponding coefficient curves. The intensity and coefficient of variation of the coefficient curves were used to analyze the synergistic strategy of the activation patterns. Representative channels were selected based on the activation patterns and the complexity of the sEMG signals of these channels was obtained using non-linear analysis.

1) Pre-Processing: Raw HD-sEMG signals were pre-processed using a 4th order Butterworth band-pass filter (20-500 Hz), an adaptive filter to remove the power-line interference and its harmonics, and a spatial filter based on principal component analysis to discard the redundant common information and measurement noise (contribution rate <0.01). After full-wave rectification, the envelopes of the preprocessed data were extracted using a zero-delay Butterworth low-pass filter (6th order, 10 Hz), and downsampled to 5000 points × 32 channels as the envelope matrix. The envelope matrix was not normalized to obtain the modulation information of the force level.

2) Synergy Extraction: The NMF algorithm has been successfully used in extracting activation patterns from HD sEMG signals [29], [40]. The NMF algorithm can be described by the following equation (1):

$$V^{m\times n} = W^{m\times s} C^{s\times n} \tag{1}$$

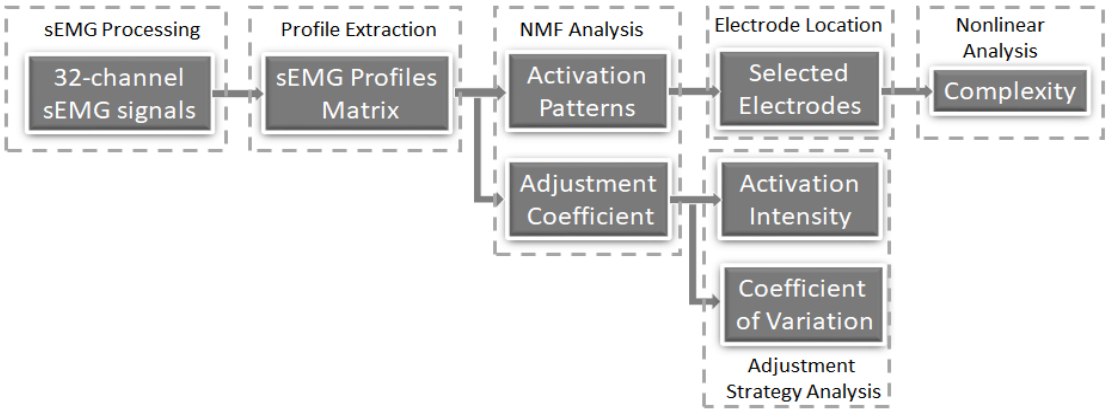

Fig. 2. Block diagram of the proposed method framework.

where, $V^{m\times n}$ represents the envelope matrix with m channels and n sample points of sEMG ($m = 32$, $n = 5000$). Each column of $W^{m\times s}$ represents an activation pattern with m weighting factors, describing the spatial organization and coordination of m channels. s is the number of activation patterns ($1 \leq s \leq$ m). Each row of Each row of $C^{s\times n}$ represents the regulation coefficients corresponding to the activation pattern, which can show the dynamically tuning process of each activation pattern over time.

The number of activation patterns needs to be selected from 1 to 32. The larger the value of s, the higher the reconstruction accuracy of the reconstruction matrix $V' = WC$. The reconstruction accuracy can be measured by the variability accounted for (VAF), as shown in equation (2):

$$V^{m\times n} = \left(1 - \frac{(V - V')^2}{V^2}\right) \times 100\% \tag{2}$$

Recent studies found that for force-specific isometric tasks, using VAF $>$ 90% as a criterion for the number of synergies may not be enough, as the residual component of the sEMG may contain crucial information about the movements [41], [42]. Thus, the threshold is set as the average VAF $>$ 95% and the increase of VAF $<$ 1% [43], [44].

3) Similarity of Activation Patterns: According to the synergy theory proposed by Bernstein, synergies as neural organizations with two functions: grouping elements to reduce motor redundancy and ensuring dynamic stability of action. Based on the first function, muscle synergies can be expressed as a few stable activation patterns (W) and are recruited with specific time-varying coefficients(C) [45], [46]. If muscle synergy exists in the EDC compartments, the corresponding spatial activation synergy patterns should be similar at the same force level, and also between different force levels. The similarity of the activation patterns of EDC obtained from the HD sEMG signals was assessed using a two-dimensional correlation coefficient ($r2$), as expressed in equation (3).

$$r2 = \frac{\sum_m \sum_n (A_{mn} - \bar{A})(B_{mn} - \bar{B})}{\sqrt{\left(\sum_m \sum_n (A_{mn} - \bar{A})^2\right)\left(\sum_m \sum_n (B_{mn} - \bar{B})^2\right)}} \tag{3}$$

where both A_{mn} and B_{mn} are m by n-dimensional matrices. $\bar{A}$ ($\bar{B}$) is the mean of all elements in matrix A (B).

4) Regulation of Activation Patterns: To investigate the regulation progress of spatial activation patterns during sustained contraction, the obtained 5000 points $\times$ 32 channels of time-varying coefficients were evenly divided into 5 periods. The RMS was used to characterize the activation intensity of spatial activation patterns:

$$RMS = \left(\frac{1}{N}\sum_{N}^{i=1} x_i^2\right)^{1/2} \tag{4}$$

N is the window length (N=1000), and x_i is the ith sample point in the window.

The volatility of the time-varying coefficients was assessed using the coefficient of variation (CV), which is calculated as:

$$CV = \frac{\sqrt{\sum_{i=1}^{N}(x_i - \bar{x})^2}}{\bar{x}} \tag{5}$$

5) Nonlinear Analysis: According to previous studies [40], 8 of all channels with high weight factors (the top 25%) of activation patterns were taken as the major contributors, which can characterize the activation patterns better. Therefore, to evaluate the nonlinearity of the activation pattern, the complexity of the representative channels of the activation patterns was assessed using fuzzy entropy (FuzzyEn). The preprocessed sEMG data of these 8 channels were divided into 5 epochs (i.e. 36000 points per segment), and the FuzzyEn of each epoch was calculated as shown in the following.

$$FuzzyEn(N, m, n, r) = \ln \Phi^m(n, r) - \ln \Phi^{m+1}(n, r) \tag{6}$$

where, the embedding dimension m is 2, the step length n is 2, and the similarity tolerance r is set to 0.25 $\times$ SD (standard deviation of the sEMG signal within a single time window). These values were suitable for obtaining the complexity of sEMG signals, based on the suggestion of Chen et al. [47]. $\Phi^m(n, r)$ is the likelihood of reconstructing the vector for a single time window sEMG signals within the tolerance r of the pattern vector. In this study, FuzzyEn was obtained by calculating $\Phi^2(n, r)$ and $\Phi^3(n, r)$ for each time window of the sEMG signals. For each pattern, 8 FuzzyEn values of 8 channels were obtained for each same epoch, and their

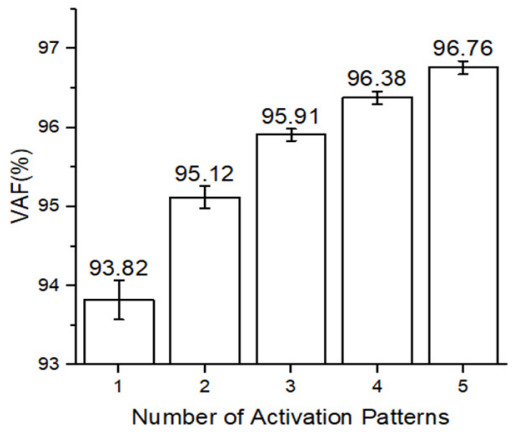

Fig. 3. Mean VAF values corresponding to the different number of activation patterns.

averaged values were calculated as the complexity for each epoch. Then, the 5 averaged FuzzyEn values were normalized to the first epoch for each trail. The mean values of normalized FuzzyEn values of three repeated trials were used to represent the final complexity of each force level.

E. Statistical Comparisons

To quantify the difference in regulation strategies across different activation patterns, forces, and epochs, a mixed line model was performed on the RMS, CV, and FuzzyEn values, with the epoch (5 levels: 1∼5) and the force (3 levels: 15%, 30%, and 45% MVC) considered as the within-subject factors and the patterns (2 levels: W1 vs. W2) considered as the between-subject factors. Repeated measures analysis of variance (ANOVA) was used to test differences in RMS, CV, and FuzzyEn analysis. In the case of significant interaction, a series of post hoc pairwise comparisons with LSD correction were conducted to compare pattern differences separately for each epoch. The significant differences were set at $p < 0.05$.

III. Results

A. The Number of Activation Patterns

The mean VAF values obtained in the NMF method of the sEMG signals from EDC are shown in Fig. 3. When the number of activation patterns s (NoS) is 1, the average value of VAF reaches 93.82%. Assuming that the NoS is 1, the spatial activation of the EDC does not change with time during isometric sustained contraction. However, this result contradicts the results of previous studies. In fact, the spatial activation of multi-tendon muscles exhibits spatial reorganization and gravity shift during sustained contraction [48]. In particular, our previous studies demonstrated that different spatial regions of the EDC exhibit differential trends with time [38]. Therefore, selecting NoS as 1 may lose certain important information in the HD sEMG signals related to finger force control, which is not appropriate. When s is 2, VAF is more than 95% and the increase is less than 1%, which meets the setting requirement. At this point, the time-varying coefficient curves of the two spatial activation patterns show different trends. If the two patterns were separated from the same one, then both should have similar time-varying activation profiles. Therefore, it is more reasonable to extract two spatial activation patterns. Here, NoS was selected as 2.

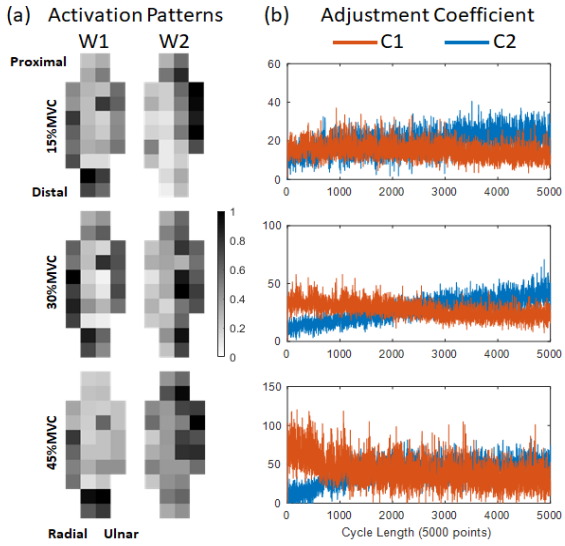

Fig. 4. (a) The two activation patterns and (b) corresponding time-varying coefficient curves of ED for sub1 at 15%, 30% and 45% MVC.

B. The Spatial Distribution of Activation Patterns and the Trends of Time-Varying Coefficients

Fig. 4 shows HD-sEMG signal decomposition results for EDC during sustained contractions from one subject, including two spatial activation patterns and corresponding coefficient curves. The weighting factors of two activation patterns are displayed in the grayscale maps, with higher weights reflecting bigger grayscale values. The spatial distribution of the weighting factors is heterogeneous for two activation patterns. The darker colored areas in the grayscale map constitute the main activation areas. The main activation areas of W1 are concentrated on the distal radial side, while those areas of W2 are located on the proximal ulnar side.

As shown in Fig. 4, C1 and C2 correspond to the time-varying coefficient curves of W1 and W2, respectively. The C1 curves (red) exhibit a downward trend, while the C2 curves (blue) exhibit a gradual upward trend.

To test the hypothesis that the composition of synergies was consistent across force levels, we performed the calculation of the correlation coefficients for the spatial activation patterns of W1 and W2, shown in Table I. According to the rule-of-thumb scale for evaluating the correlation coefficient, correlations of 0.7 to 0.89 are high correlation [49]. Therefore, the activation patterns showed high correlation coefficients between different trials at the same force level and between different force levels, indicating that the spatial structures of the synergy patterns of EDC compartments are stable, and independent of trial and force level.

C. Comparison With Respect to Activation Intensity and Variability

To explore the time dependence of the intensity and variability of the synergy signal, we calculated the RMS and CV values of coefficient curves for the five epochs.

TABLE I
CORRELATION (MEAN±SD) BETWEEN SYNERGY PATTERNS AT SAME FORCE LEVELS AND DIFFERENT FORCE LEVELS

Synergy	Same force levels (MVC)			Different force levels (MVC)		
	15% & 15%	30% & 30%	45% & 45%	15% & 30%	15% & 45%	30% & 45%
W1	0.840 ± 0.112	0.919 ± 0.049	0.830 ± 0.109	0.855 ± 0.032	0.805 ± 0.082	0.864 ± 0.074
W2	0.819 ± 0.117	0.906 ± 0.043	0.858 ± 0.071	0.809 ± 0.103	0.799 ± 0.076	0.875 ± 0.051

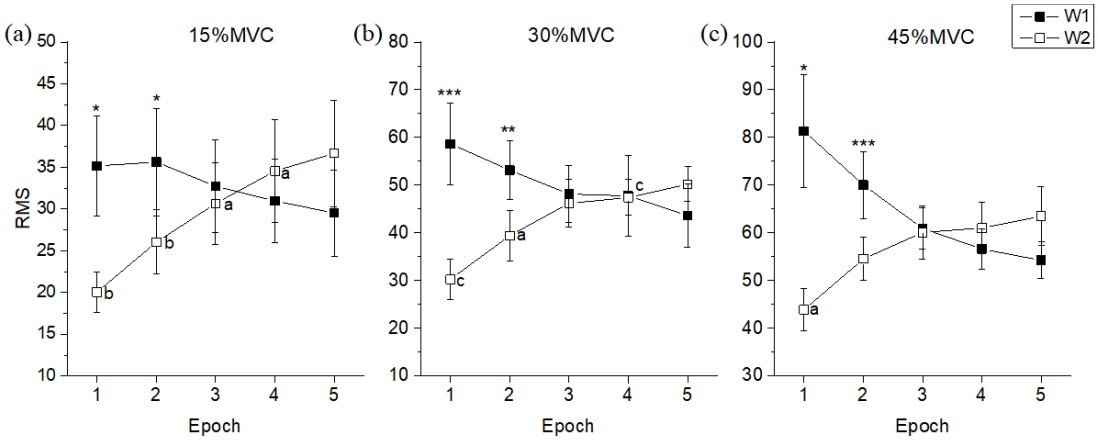

Fig. 5. RMS values of two activation patterns for five epochs at three force levels. (a) 15% MVC, (b) 30% MVC, (c) 45% MVC. Asterisks indicate significant difference between activation patterns $^{*}p < 0.05$; $^{**}p < 0.01$; $^{***}p < 0.005$. Lowercase letters indicate significant differences $^{a}p < 0.05$; $^{b}p < 0.01$; ^{c} $p < 0.005$ among epochs.

TABLE II
RESULTS OF THE POST HOT T-TEST ON RMS OF W2 BETWEEN THE 5TH EPOCH AND THE OTHER EPOCHS (1ST TO 4TH)

Force	p value			
	1st	2nd	3rd	4th
15% MVC	**0.009**^{b}	**0.009**^{b}	**0.018**^{a}	**0.038**^{a}
30% MVC	**0.001**^{c}	**0.011**^{b}	0.148	**0.005**^{c}
45% MVC	**0.010**^{a}	0.092	0.431	0.390

The RMS results of the coefficient curves were shown in Fig.5. The RMS values of C1 decreased with time, while that of C2 increased. The three-way repeated measured ANOVA analysis reported no significant interaction among all three factors, while a significant interaction between pattern and epoch ($F(1.7171,9.366) = 12.758$, $p = 0.005$). During 1st and 2nd epochs, the RMS values of C2 were significant lower than that of C1 at each force level (15%MVC: 1st, $p = 0.010$, 2nd, $p = 0.034$; 30%MVC: 1st, $p = 0.002$, 2nd, $p = 0.007$; 45%MVC: 1st, $p = 0.011$, 2nd, $p = 0.004$).

The *post hoc t-test* revealed a significant RMS increase with epochs for W2. The 5th epoch yielded higher RMS than other periods, p values were shown in Table II. Moreover, force had a significant effect on RMS values for both W1 ($F(2,16) = 48.210$, $p < 0.001$) and W2 ($F(1.111,8.884) = 25.356$, $p = 0.001$). The RMS values increased with force (W1: 15% vs. 30%MVC, $p = 0.001$; 30% vs. 45%MVC, $p = 0.004$; W2: 15% vs. 30%MVC, $p < 0.001$; 30% vs. 45%MVC, $p = 0.006$).

The CV values of time-varying coefficient curves of two activation patterns are shown in Fig. 6. Results of ANOVA analysis for CV values revealed no significant interaction among all three factors. However, a significant interaction between pattern and epoch ($F(1.302,10.414) = 22.426$, $p < 0.001$). Individual effects analysis showed significant effects of patterns on CV at each force level. For 15% MVC, the CV of C1 was significantly lower than that of C2 ($p < 0.001$) at the beginning (1st epoch), as the CV of C1 increased and that of C2 decreased simultaneously, while the CV of C2 was significantly lower than C1 in the 5th epoch ($p < 0.001$). For 30% and 45% MVC, the CV value of C2 was close to that of C1 in the initial stage(1st to 2nd epochs) and significantly lower in the latter stage (3rd to 5th epochs).

Individual effects analysis also showed epoch has significant effects on CV at each force level. For W1, CV values of C1 were increased with epoch (15%MVC, $F(1.441,11.531) = 10.283$, $p = 0.005$; 30%MVC, $F(1.348,10.783) = 9.148$, $p = 0.008$; 45%MVC, $F(1.600,12.797) = 11.887$, $p = 0.002$). Further post hoc comparisons showed the CV values of the 5th epoch were significantly higher than the 1stto 3rd epochs (Table III). For C2, CV values exhibited inclined trend with epochs(15%MVC, $F(1.301,10.411) = 14.458$, $p = 0.002$; 30%MVC, $F(1.253,10.027) = 10.751$, $p = 0.006$; 45%MVC, $F(1.297,10.373) = 5.806$, $p = 0.030$). For different force levels, the CV values of the 5th epoch were found significantly lower than other epochs, with 1st to 4th, 1st to 2nd, and 1st epochs at 15%, 30%, and 45% MVC, respectively, which indicated the declining trend slowed down.

D. Relationship of Intensity and Stability

To further explore the synergy of the two activation patterns, the correlation coefficients of the two synergies were

TABLE III
RESULTS OF THE POST HOC T-TEST FOR CV BETWEEN THE 5TH EPOCH AND THE OTHER EPOCHS (1ST TO 4TH)

Force	*p* value of W1				*p* value of W2			
	1st	2nd	3rd	4th	1st	2nd	3rd	4th
15% MVC	**0.007**[b]	**0.012**[a]	**0.012**[a]	0.165	**0.003**[c]	**0.015**[a]	**0.043**[a]	**0.030**[a]
30% MVC	**0.007**[b]	**0.032**[a]	**0.033**[a]	**0.031**[a]	**0.007**[b]	**0.007**[b]	0.062	0.066
45% MVC	**0.003**[c]	**0.005**[c]	**0.003**[c]	0.082	**0.047**[a]	0.203	0.862	0.427

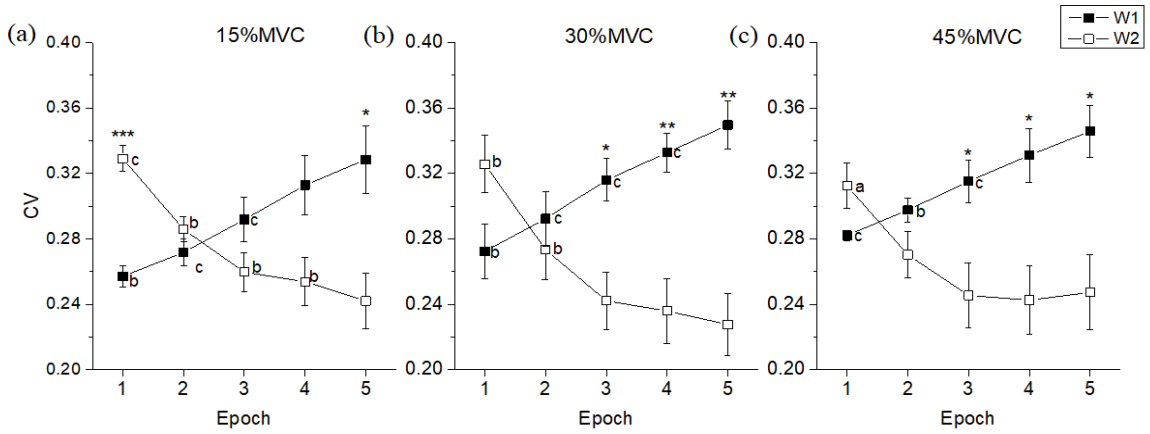

Fig. 6. CV values analysis in each of two activation patterns for five epochs and three force levels. (a) 15% MVC, (b) 30% MVC, (c) 45% MVC. Asterisks indicate significant difference between activation patterns $^{*}p < 0.05$; $^{**}p < 0.01$; $^{***}p < 0.005$. Lowercase letters indicate significant differences $^{a}p < 0.05$; $^{b}p < 0.01$; $^{c}p < 0.005$ among epochs.

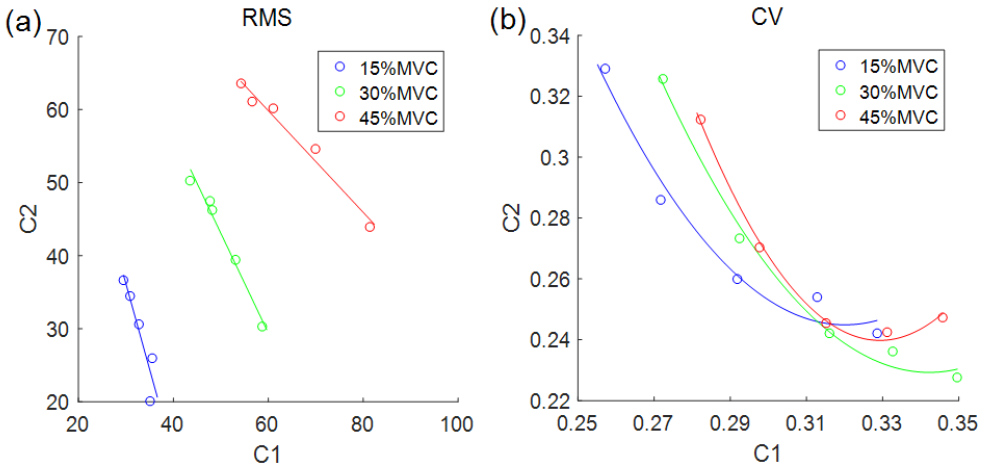

Fig. 7. Fitting results of RMS (a) and CV (b) between C1 and C2 at three force levels.

calculated for the RMS and CV of the activation coefficients at each force level. As Table IV shown, both RMS and CV values showed a negative and high correlation between C1 and C2 at all three force levels.

To investigate the relationship between the two activation patterns, RMS and CV were fitted using linear and quadratic functions, respectively. Fig. 7a shows a linear relationship between the RMS of C1 and C2. The absolute value of the slopes of the fitted straight line decreases as the force increases (15%MVC, 2.345; 30%MVC, 1.366; 45%MVC, 0.696). However, Fig. 7b shows the CVs of C1 and C2 having a quadratic relationship. Combined with Fig. 6, it can be seen that there is an overall decreasing trend in the CV of C2 as the CV of C1 increases, and this decreasing trend is slowing down. Even at 45% MVC, the CV of C2 at the maximum CV of C1 shows a slight increase compared to the adjacent points.

E. Comparison With Respect to Complexity

The normalized FuzzyEn results for the representative channels corresponding to the main contribution zones are shown in Fig. 8. The three-way repeated-measures ANOVA for the normalized FuzzyEn showed no significant interactions among the three factors as well. Two-way repeated-measures

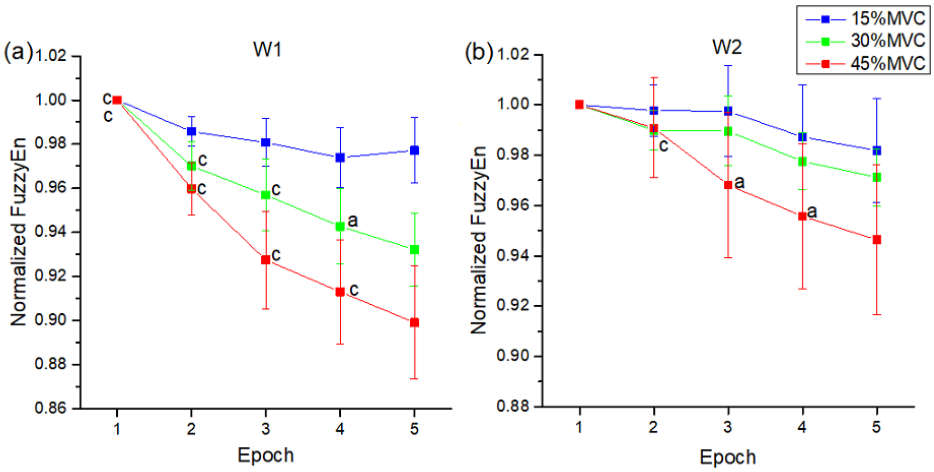

Fig. 8. Normalized FuzzyEn of epochs at three force levels (15%, 30%, and 45% MVC) for W1 (a) and W2 (b). Lowercase letters indicate significant differences a $p < 0.05$; b $p < 0.01$; c $p < 0.005$ among epochs.

TABLE IV
CORRELATION OF RMS AND CV VALUES BETWEEN TWO COEFFICIENT CURVES AT THREE FORCE LEVELS

Force	15% MVC	30% MVC	45% MVC
RMS	-0.921	-0.989	-0.987
CV	-0.927	-0.940	-0.856

ANOVA revealed significant interactions between force and epoch ($F(2.086,16.663) = 4.789$, $p = 0.022$). However, no significant interactions between pattern and epoch or force were reported, which indicated pattern had no significant effect on FuzzyEn.

Significant effects of epochs on FuzzyEn values were found for both patterns at higher force levels (Table V). The FuzzyEn significantly decreased with epoch for W1 at 30% ($F(1.283,10.261) = 11.747$, $p = 0.004$) and 45% MVC ($F(1.196,9.571) = 12.984$, $p = 0.004$), but for W2 at 45% MVC ($F(4,32) = 3.070$, $p = 0.030$).

IV. DISCUSSION

To investigate coordination strategies of EDC compartments, this study utilized the NMF method to characterize the spatial distribution of the activation regions and coordination process for instructed and non-instructed fingers during index finger sustained contraction. The results showed that two activation patterns and coefficient curves were extracted from HD sEMG signals in EDC muscle during the tasks. The two activation patterns exhibited specific lateralized spatial distribution, and the time-varying adjustment process of corresponding coefficient curves could efficiently depict the coordination strategy of EDC compartments during the index finger with a sustained constant isometric extension.

A. Stable Spatial Activation Patterns

As the results of the NMF analysis in Fig. 3 shown, the VAF has reached 95.12% when the number of S is 2, and the increase satisfies <1%. This implies that two activation patterns are obtained from the EDC compartments during sustained constant force extension of the index finger. Fig. 4a shows that the spatial distribution of both activation patterns is heterogeneous. The primary activation area of the instructed finger activation pattern (W1, named primary pattern) was located on the distal radial side, and the primary activation area of the non-task finger activation pattern (W2, named auxiliary pattern) was demonstrated that the weighting factors for each activation pattern are highly correlated and are independent of force and trial. This implies that similar to muscle synergy, the spatial distribution of the obtained activation patterns is stable, verifying the existence of compartment coordination in multi-tendon muscles. For the coefficient curves corresponding to the activation patterns in Fig. 4b and Fig. 5, at the initial stage, the activation intensity of the primary pattern was higher and that of the auxiliary pattern was lower. This is consistent with the results of previous studies that, for multi-tendon muscles, the intended compartments are predominantly activated and the spatial regionalization of muscle activity is more evident [37].

These results demonstrate our first hypothesis that there are synergy patterns among EDC compartments corresponding to instructed and non-instructed fingers during single-finger extension, reflecting coordinated strategies in non-independent EDC compartments to simplify the CNS control variables.

B. The Intensity and Stability Compensations of the Auxiliary Pattern

Previous studies have confirmed that the synergy coefficient curves of activation patterns extracted from sEMG signals are reflections of central driving, which implies the tuning strategy for synergy patterns [46]. Therefore, in this study, the RMS and CV of the coefficient curve were used to quantitatively evaluate the activation intensity and volatility of the activation patterns, and found significantly different regulatory processes and a close cooperative relationship between them.

The RMS results (Fig. 5) showed that the two activation patterns were activated simultaneously, even during the initial

TABLE V
RESULTS OF THE POST HOC T-TEST FOR FUZZYEN BETWEEN THE 5TH EPOCH AND THE OTHER EPOCHS(1ST-4TH)

Force	Significance (p values)							
	W1				W2			
	1st	2nd	3rd	4th	1st	2nd	3rd	4th
15% MVC	0.166	0.394	0.492	0.321	0.402	0.248	0.110	0.181
30% MVC	**0.003**[c]	**0.001**[c]	**0.001**[c]	**0.032**[a]	**0.034**[a]	0.147	0.072	0.133
45% MVC	**0.004**[c]	**0.004**[c]	**0.004**[c]	**0.005**[c]	0. 056	**0.003**[c]	**0.016**[a]	**0.039**[a]

epochs of low force levels the auxiliary pattern had been already activated. It demonstrated that the compartments of a multi-tendon muscle have non-independent activation properties during sustained force output, which is due to complex physiological connections and neural co-inputs among the compartments [37]. However, the activation intensity of the two patterns showed different change processes over time: the activation intensity of the primary pattern with higher activation at the beginning showed a decreasing trend; while the auxiliary pattern with lower activation intensity at the beginning showed a significant increase in activation intensity, and even approached the activation intensity of the primary pattern at the later stages. It suggested that the auxiliary pattern played an increasingly important compensation role during sustained contraction, rather than being enslaved [50]. Further correlation analysis showed a strong negative correlation between the activation intensity of the two patterns at all three force levels. This negative covariance might be similar to the error compensation observed in multi-finger force synergies, which was considered to be an essential feature of the motion synergy effect. It is known that the intensity of sEMG activity is generally proportional to muscle force output in a non-fatigued state [51], [52]. Therefore, on the one hand, the slight reduction in the activation intensity of the primary pattern caused a decrease in the force output of this pattern. On the other hand, the activation intensity of the auxiliary pattern increased significantly can lead to an increase in non-instructed finger force output, which was consistent with the results of previous mechanistic studies [53], [54], [55]. These studies have documented, during continuous force production, a consistent increase in the force output of non-instructed fingers with time under feedback on the primary finger force. So the increased force output of the auxiliary pattern compensates for the loss of force in the primary pattern [50] and then maintains the whole output force at the required level. These results demonstrate our second hypothesis that the two stable patterns were recruited by different coordination control strategies during the index finger sustained contraction.

The CV results (Fig. 6) suggest that the trend of stability change in both patterns is a specific process: the volatility of the primary pattern and the auxiliary pattern significantly increased and decreased, respectively, and those are not affected by force level. In the early stages, the primary pattern volatility was lower, but the volatility of the auxiliary pattern is significantly lower than that of the primary pattern. The reduced volatility of the auxiliary pattern assists the primary pattern in achieving overall stability, which is a manifestation of synergy [56], allowing for stability of index finger posture and force. The high negative correlations of the CVs (Table III) further confirm the existence of the stability compensation effect of the auxiliary pattern, and also further demonstrates our second hypothesis. This is consistent with previous research finding that a typical strategy for achieving force stability is a result of negative co-variation between patterns [57]. This compensation is presumed to be an additional important manifestation of compartment coordination. Furthermore, the fit results for RMS and CV between C1 and C2 are linear and quadratic, respectively, indicating that these two compensations are different (Fig. 7). This is consistent with previous findings using a mechanical model, where the CNS achieves control of force strength and stability through two neural variables [21].

Therefore, during sustained constant extension of the index finger, there is a close synergistic relationship between the primary pattern and the auxiliary pattern, which is manifested as the intensity and stability compensation of the auxiliary pattern for the primary pattern. These two compensations could be seen as coarse and fine tuning processes to secure constant finger force, and are the manifestation of multi-compartment synergy at different control levels.

It is worth noting that both compensations are limited. On the one hand, intensity compensation capacity decreases when the force increases from 15% to 45% MVC (Fig. 5), which could be further verified by the slight downward trend in the slope of the fitted line between the RMS of C1 and C2 (Fig. 7a). On the other hand, a significant reduction in the stability compensation of the auxiliary pattern at later stages of high force level (45% MVC), that is, the CV of C2 decreases slowly in the later periods (Fig. 6). This conclusion is also verified by the quadratic relationship between C1 and C2 (Fig. 7b). Therefore, the intensity and stability compensations of the auxiliary pattern are limited, and these compensations become weaker at high force levels. For the neuromuscular physiological system, the ability to achieve compensation for maintaining a constant force as an adaptive response is limited. Based on previous research, complexity is related to the ability of this adaptive response. FuzzyEn characterizing the complexity has been successfully used as a measure of the adaptive capacity of a neuromuscular physiological system [58]. In this study, the FuzzyEn of the auxiliary pattern

showed a decreasing trend (Fig. 8). Therefore, this loss of complexity is thought to be associated with a reduced adaptive capacity [59].

In addition, this intensity compensation of the activation patterns can be applied to explain the gravity shift and spatial reorganization phenomenon in multi-tendons during sustained contraction, which has been reported in previous studies [48]. During sustained contraction, although the structure of the two patterns is stable, the intensity of their time-varying coefficients is negatively correlated. The cooperation of the two activation patterns causes changes in overall spatial distribution, showing spatial reorganization and a shift in the gravity center of topographic maps. Therefore, the results of this study indicate that these phenomena (gravity shift and spatial reorganization) can be considered as performances of the compartment synergy in multi-tendons.

C. Limitations and Future Work

Our experiments currently involved only a single-finger extension task for the index finger. Independent extension tasks for the other three fingers (middle, ring, and little fingers) should be included in future studies to verify whether this synergy strategy exists in these cases. Our findings showed that both compensations of the auxiliary pattern slow down at high force levels, which implied the support of the auxiliary pattern for the task pattern maybe not be infinite during sustained contraction. Therefore, future experiments should also be extended to induce fatigue, to explore the effect of fatigue on the control strategy of CNS.

V. Conclusion

The present study investigated the control strategies of CNS on multi-tendon muscles during sustained contraction, and found during sustained extension of the index finger, the primary pattern and the auxiliary pattern of the EDC were lateralized and corresponded to the index finger part and other parts of the EDC, respectively. Both RMS and CV values of the coefficient curves between the two activation patterns showed negative correlations, indicating that to maintain a stable force output, two compensations of the auxiliary pattern were employed to assist the primary pattern in term of intensity and stability. These results provide a new perspective to reveal the synergy strategies of EDC compartments during index finger sustained contraction and a new approach for constant force control of prosthetic hands.

Acknowledgment

The authors much appreciated the subjects for participating in this study.

References

[1] A. R. Sobinov and S. J. Bensmaia, "The neural mechanisms of manual dexterity," *Nature Rev. Neurosci.*, vol. 22, no. 12, pp. 741–757, Dec. 2021.

[2] M. Santello, G. Baud-Bovy, and H. Jörntell, "Neural bases of hand synergies," *Frontiers Comput. Neurosci.*, vol. 7, pp. 7–23, Apr. 2013.

[3] N. van Beek, D. F. Stegeman, J. C. van den Noort, D. H. E. J. Veeger, and H. Maas, "Activity patterns of extrinsic finger flexors and extensors during movements of instructed and non-instructed fingers," *J. Electromyogr. Kinesiol.*, vol. 38, pp. 187–196, Feb. 2018.

[4] F. J. Valero-Cuevas, J. W. Yi, D. Brown, R. V. McNamara, C. Paul, and H. Lipson, "The tendon network of the fingers performs anatomical computation at a macroscopic scale," *IEEE Trans. Biomed. Eng.*, vol. 54, no. 6, pp. 1161–1166, Jun. 2007.

[5] D. A. Keen and A. J. Fuglevand, "Common input to motor neurons innervating the same and different compartments of the human extensor digitorum muscle," *J. Neurophysiol.*, vol. 91, no. 1, pp. 57–62, Jan. 2004.

[6] C. Dai, H. Shin, B. Davis, and X. Hu, "Origins of common neural inputs to different compartments of the extensor digitorum communis muscle," *Sci. Rep.*, vol. 7, no. 1, pp. 1–11, Oct. 2017.

[7] H. Van Duinen, W. S. Yu, and S. C. Gandevia, "Limited ability to extend the digits of the human hand independently with extensor digitorum," *J. Physiol.*, vol. 587, no. 20, pp. 4799–4810, Oct. 2009.

[8] J. N. A. L. Leijnse, "Measuring force transfers in the deep flexors of the musician's hand: Theoretical analysis, clinical examples," *J. Biomech.*, vol. 30, no. 9, pp. 873–882, Sep. 1997.

[9] S. Reschechtko, V. M. Zatsiorsky, and M. L. Latash, "The synergic control of multi-finger force production: Stability of explicit and implicit task components," *Exp. Brain Res.*, vol. 235, no. 1, pp. 1–14, Jan. 2017.

[10] M. B. Carpenter, "The co-ordination and regulation of movements," *J. Neuropathol. Experim. Neurol.*, vol. 27, no. 2, p. 348, Apr. 1968.

[11] A. d'Avella, P. Saltiel, and E. Bizzi, "Combinations of muscle synergies in the construction of a natural motor behavior," *Nature Neurosci.*, vol. 6, pp. 300–308, Mar. 2003.

[12] Z. X. Gao et al., "Synergistic recruitment of multi-scale myoelectric oscillations of upper limb during infant crawling," in *Proc. 40th Annu. Int. Conf. IEEE Eng. Med. Biol. Soc. (EMBC)*, Jul. 2018, pp. 5966–5969.

[13] M. Santello et al., "Hand synergies: Integration of robotics and neuroscience for understanding the control of biological and artificial hands," *Phys. Life Rev.*, vol. 17, pp. 1–23, Jul. 2016.

[14] S. Tanzarella, S. Muceli, A. Del Vecchio, A. Casolo, and D. Farina, "Non-invasive analysis of motor neurons controlling the intrinsic and extrinsic muscles of the hand," *J. Neural Eng.*, vol. 17, no. 4, Aug. 2020, Art. no. 046033.

[15] S. Tanzarella, S. Muceli, M. Santello, and D. Farina, "Synergistic organization of neural inputs from spinal motor neurons to extrinsic and intrinsic hand muscles," *J. Neurosci.*, vol. 41, no. 32, pp. 6878–6891, Aug. 2021.

[16] S. Madarshahian, J. Letizi, and M. L. Latash, "Synergic control of a single muscle: The example of flexor digitorum superficialis," *J. Physiol.*, vol. 599, no. 4, pp. 1261–1279, Feb. 2021.

[17] S. Madarshahian and M. L. Latash, "Synergies at the level of motor units in single-finger and multi-finger tasks," *Exp. Brain Res.*, vol. 239, no. 9, pp. 2905–2923, Sep. 2021.

[18] Z. M. Li, V. M. Zatsiorsky, and M. L. Latash, "Contribution of the extrinsic and intrinsic hand muscles to the moments in finger joints," *Clin. Biomech.*, vol. 15, no. 3, pp. 203–211, Mar. 2000.

[19] V. M. Zatsiorsky, Z.-M. Li, and M. L. Latash, "Enslaving effects in multi-finger force production," *Exp. Brain Res.*, vol. 131, no. 2, pp. 187–195, Mar. 2000.

[20] M. L. Latash, Z.-M. Li, and V. M. Zatsiorsky, "A principle of error compensation studied within a task of force production by a redundant set of fingers," *Exp. Brain Res.*, vol. 122, no. 2, pp. 131–138, Sep. 1998.

[21] S. Li, M. L. Latash, and V. M. Zatsiorsky, "Finger interaction during multi-finger tasks involving finger addition and removal," *Exp. Brain Res.*, vol. 150, no. 2, pp. 230–236, May 2003.

[22] M. Latash, J. Scholz, F. Danion, and G. Schöner, "Structure of motor variability in marginally redundant multifinger force production tasks," *Exp. Brain Res.*, vol. 141, no. 2, pp. 153–165, Nov. 2001.

[23] M. L. Latash, *Synergy*. London, U.K.: Oxford Univ. Press, 2008.

[24] L.-C. Kuo, S.-W. Chen, C.-J. Lin, W.-J. Lin, S.-C. Lin, and F.-C. Su, "The force synergy of human digits in static and dynamic cylindrical grasps," *PLoS ONE*, vol. 8, no. 3, Mar. 2013, Art. no. e60509.

[25] J. K. Shim, H. Olafsdottir, V. M. Zatsiorsky, and M. L. Latash, "The emergence and disappearance of multi-digit synergies during force-production tasks," *Expe. Brain Res.*, vol. 164, no. 2, pp. 260–270, Jul. 2005.

[26] M. Shinohara, S. Li, N. Kang, V. M. Zatsiorsky, and M. L. Latash, "Effects of age and gender on finger coordination in MVC and submaximal force-matching tasks," *J. Appl. Physiol.*, vol. 94, no. 1, pp. 259–270, Jan. 2003.

[27] M. Tagliabue, A. L. Ciancio, T. Brochier, S. Eskiizmirliler, and M. A. Maier, "Differences between kinematic synergies and muscle synergies during two-digit grasping," *Frontiers Hum. Neurosci.*, vol. 9, p. 165, Mar. 2015.

[28] M. H. Schwartz, A. Rozumalski, and K. M. Steele, "Muscle synergy complexity is related to selective motor control in cerebral palsy," *Gait Posture*, vol. 39, p. S40, Jun. 2014.

[29] A. d'Avella, A. Portone, L. Fernandez, and F. Lacquaniti, "Control of fast-reaching movements by muscle synergy combinations," *J. Neurosci.*, vol. 26, no. 30, pp. 7791–7810, Jul. 2006.

[30] A. Ebied, E. Kinney-Lang, L. Spyrou, and J. Escudero, "Evaluation of matrix factorisation approaches for muscle synergy extraction," *Med. Eng. Phys.*, vol. 57, pp. 51–60, Jul. 2018.

[31] D. Staudenmann, D. F. Stegeman, and J. H. van Dieën, "Redundancy or heterogeneity in the electric activity of the biceps Brachii muscle? Added value of PCA-processed multi-channel EMG muscle activation estimates in a parallel-fibered muscle," *J. Electromyography Kinesiol.*, vol. 23, no. 4, pp. 892–898, 2013.

[32] J. N. A. L. Leijnse, S. Carter, A. Gupta, and S. McCabe, "Anatomic basis for individuated surface EMG and homogeneous electrostimulation with neuroprostheses of the extensor digitorum communis," *J. Neurophysiol.*, vol. 100, no. 1, pp. 64–75, Jul. 2008.

[33] C. Huang, X. Chen, S. Cao, and X. Zhang, "Muscle-tendon units localization and activation level analysis based on high-density surface EMG array and NMF algorithm," *J. Neural Eng.*, vol. 13, no. 6, Dec. 2016, Art. no. 066001.

[34] C. Dai and X. Hu, "Extracting and classifying spatial muscle activation patterns in forearm flexor muscles using high-density electromyogram recordings," *Int. J. Neural Syst.*, vol. 29, no. 1, Feb. 2019, Art. no. 1850025.

[35] M. Rojas-Martínez, L. Y. Serna, M. Jordanic, H. R. Marateb, R. Merletti, and M. Á. Mañanas, "High-density surface electromyography signals during isometric contractions of elbow muscles of healthy humans," *Scientific Data*, vol. 7, no. 1, pp. 1–12, Nov. 2020.

[36] X. Chen, S. Wang, C. Huang, S. Cao, and X. Zhang, "ICA-based muscle–tendon units localization and activation analysis during dynamic motion tasks," *Med. Biol. Eng. Comput.*, vol. 56, no. 3, pp. 341–353, Mar. 2018.

[37] X. Hu, N. L. Suresh, C. Xue, and W. Z. Rymer, "Extracting extensor digitorum communis activation patterns using high-density surface electromyography," *Frontiers Physiol.*, vol. 6, p. 279, Oct. 2015.

[38] Z. Gao et al., "Spatial reorganization of myoelectric activities in extensor digitorum for sustained finger force production," *Sensors*, vol. 19, no. 3, p. 555, Jan. 2019.

[39] J. Roh, W. Z. Rymer, and R. F. Beer, "Robustness of muscle synergies underlying three-dimensional force generation at the hand in healthy humans," *J. Neurophysiol.*, vol. 107, no. 8, pp. 2123–2142, Apr. 2012.

[40] C. Huang, X. Chen, S. Cao, B. Qiu, and X. Zhang, "An isometric muscle force estimation framework based on a high-density surface EMG array and an NMF algorithm," *J. Neural Eng.*, vol. 14, no. 4, Aug. 2017, Art. no. 046005.

[41] V. R. Barradas, J. J. Kutch, T. Kawase, Y. Koike, and N. Schweighofer, "When 90% of the variance is not enough: Residual EMG from muscle synergy extraction influences task performance," *J. Neurophysiol.*, vol. 123, no. 6, pp. 2180–2190, Jun. 2020.

[42] N. A. Turpin, S. Uriac, and G. Dalleau, "How to improve the muscle synergy analysis methodology?" *Eur. J. Appl. Physiol.*, vol. 121, no. 4, pp. 1009–1025, Apr. 2021.

[43] H. V. Nguyen Sy, I. Nambu, and Y. Wada, "The adjustment of muscle synergy recruitment by controlling muscle contraction during the reaching movement," in *Proc. IEEE Int. Conf. Syst., Man, Cybern. (SMC)*, Oct. 2016, pp. 756–761.

[44] L. Tang, F. Li, S. Cao, X. Zhang, D. Wu, and X. Chen, "Muscle synergy analysis in children with cerebral palsy," *J. Neural Eng.*, vol. 12, no. 4, Aug. 2015, Art. no. 046017.

[45] P. A. Ortega-Auriol, T. F. Besier, W. D. Byblow, and A. J. C. Mcmorland, "Fatigue influences the recruitment, but not structure, of muscle synergies," *Frontiers Hum. Neurosci.*, vol. 12, p. 217, Jun. 2018.

[46] A. Gallina, S. J. Garland, and J. M. Wakeling, "Identification of regional activation by factorization of high-density surface EMG signals: A comparison of principal component analysis and non-negative matrix factorization," *J. Electromyogr. Kinesiol.*, vol. 41, pp. 116–123, Aug. 2018.

[47] W. Chen, Z. Wang, H. Xie, and W. Yu, "Characterization of surface EMG signal based on fuzzy entropy," *IEEE Trans. Neural Syst. Rehabil. Eng.*, vol. 15, no. 2, pp. 266–272, Jun. 2007.

[48] C. A. Mista, S. E. Salomoni, and T. Graven-Nielsen, "Spatial reorganisation of muscle activity correlates with change in tangential force variability during isometric contractions," *J. Electromyogr. Kinesiol.*, vol. 24, no. 1, pp. 37–45, Feb. 2014.

[49] A. G. Asuero, A. Sayago, and A. González, "The correlation coefficient: An overview," *Crit. Rev. Anal. Chem.*, vol. 36, no. 1, pp. 41–59, 2006.

[50] J. R. Martin, M. L. Latash, and V. M. Zatsiorsky, "Interaction of finger enslaving and error compensation in multiple finger force production," *Exp. Brain Res.*, vol. 192, no. 2, pp. 293–298, Jan. 2009.

[51] G. C. Ray and S. K. Guha, "Relationship between the surface EMG and muscular force," *Med. Biol. Eng. Comput.*, vol. 21, no. 5, pp. 579–586, 1983.

[52] D. Farina et al., "The extraction of neural information from the surface EMG for the control of upper-limb prostheses: Emerging avenues and challenges," *IEEE Trans. Neural Syst. Rehabil. Eng.*, vol. 22, no. 4, pp. 797–809, Jul. 2014.

[53] V. Abolins, A. Stremoukhov, C. Walter, and M. L. Latash, "On the origin of finger enslaving: Control with referent coordinates and effects of visual feedback," *J. Neurophysiol.*, vol. 124, no. 6, pp. 1625–1636, Dec. 2020.

[54] J. Ricotta, C. Cuadra, J. S. Evans, and M. L. Latash, "Perturbation-induced fast drifts in finger enslaving," *Exp. Brain Res.*, vol. 239, no. 3, pp. 891–902, Mar. 2021.

[55] J. Hirose, C. Cuadra, C. Walter, and M. L. Latash, "Finger interdependence and unintentional force drifts: Lessons from manipulations of visual feedback," *Hum. Movement Sci.*, vol. 74, Dec. 2020, Art. no. 102714.

[56] D. B. Murillo, R. S. Solana, F. J. Vera-Garcia, N. G. Fuertes, and F. J. Moreno, "Effect of increasing difficulty in standing balance tasks with visual feedback on postural sway and EMG: Complexity and performance," *Hum. Movement Sci.*, vol. 31, no. 5, pp. 1224–1237, Oct. 2012.

[57] J. Park and D. Xu, "Multi-finger interaction and synergies in finger flexion and extension force production," *Frontiers Hum. Neurosci.*, vol. 11, p. 318, Jun. 2017.

[58] L. A. Lipsitz, "Dynamics of stability: The physiologic basis of functional health and frailty," *Journals Gerontology Ser. A, Biol. Sci. Med. Sci.*, vol. 57, no. 3, pp. B115–B125, Mar. 2002.

[59] B. Manor et al., "Physiological complexity and system adaptability: Evidence from postural control dynamics of older adults," *J. Appl. Physiol.*, vol. 109, no. 6, pp. 1786–1791, Dec. 2010.